
Article:
Liu, X., Zhou, H., Lai, Y. orcid.org/0000-0002-9987-0975 et al. (1 more author) (2023) Characterisations of self-excited nonlinear oscillations at varied system parameters in a Rijke tube with a premixed laminar flame. Experimental Thermal and Fluid Science, 146. 110923. ISSN: 0894-1777

https://doi.org/10.1016/j.expthermflusci.2023.110923

Experimental Thermal and Fluid Science 146 (2023) 110923

Contents lists available at ScienceDirect

Experimental Thermal and Fluid Science

journal homepage: www.elsevier.com/locate/etfs

Characterisations of self-excited nonlinear oscillations at varied system parameters in a Rijke tube with a premixed laminar flame

Xuanqi Liu [a], Hangxu Zhou [a], Yufeng Lai [b], Yang Zhang [a,*]

[a] Department of Mechanical Engineering, The University of Sheffield, Sheffield S1 3JD, United Kingdom
[b] Department of Electronic and Electrical Engineering, The University of Sheffield, Sheffield S1 3JD, United Kingdom

ARTICLE INFO

Keywords:
Thermoacoustics
Combustion instability
Rijke tube
Nonlinear system
Recurrence analysis

ABSTRACT

Thermoacoustic instability has been one of the major concerns in various industrial combustion systems, such as Rich burn, Quick mix, Lean burn engine and aerospace engines. The complex interactions between heat release and pressure fluctuations could generate thermoacoustic oscillations with high amplitudes and frequencies in a combustion chamber, which causes many combustion problems even severe structural damage. The studies about the effects of various system parameters on thermoacoustic instability would be important due to their crucial roles in characterising the system oscillations. In this study, the effects of different system parameters in a Rijke tube, including equivalence ratio, methane flowrate, burner position and tube inner diameter, have been investigated. The time-domain analysis methods, including both phase space analysis constructed from the time-delayed method and recurrence analysis, have been conducted to explore the system characteristics under different system parameters. Furthermore, the Recurrence Quantitative Analysis (RQA) and Wayland translation error have been processed to quantify the system nonlinearity. The study has shown the effects of system parameters on system frequency response, deterministic nature and nonlinear dynamics. The system oscillation tends to be more complex and unstable when the burner is moved to lower positions or in a large diameter tube. The phase space and recurrence analysis are found to be efficient for characterising the system nonlinearity with useful insights of self-excited thermoacoustic oscillations.

1. Introduction

Self-excited thermoacoustic oscillation can be triggered in various systems, including thermoacoustic heat engines and several types of combustors [1–5]. As a challengeable yet important problem, it strongly enhances the combustion instability in the combustion systems [6–12]. For the combustion systems with enclosed combustion areas, such as gas turbine engines and rocket engines, the intense oscillation could be negative for the performance of combustors, resulting in a low efficient combustion process and even structural damage [11,13]. Therefore, predicting and controlling of thermoacoustic instabilities in the combustion systems could be critical.

Rayleigh revealed the trigger mechanism of thermoacoustic oscillation, which is the interactions between fluctuations of unsteady heat release and pressure when they are in-phase [14]. And it had been proved that this coupling effect was highly nonlinear [15]. The triggered self-excited oscillation presents a combination of linearity and nonlinearity during the developing process [16]. The self-excited thermoacoustic oscillation generally becomes nonlinear from oscillation properties [8] and system state bifurcation [9] when the oscillation is fully developed.

Combustion-induced thermoacoustic instabilities are attributed to the complex combustion-acoustic-flow interactions with the existence of combustion instabilities [12,17]. The potential control methods can be provided by exploring these complex interactions. In order to realise complex nonlinear thermoacoustic systems in lab-scale, the Rijke tube is one of the typical setups for triggering thermoacoustic oscillations [12]. Numbers of investigations have been conducted to study the characteristics of nonlinear oscillations in the Rijke tube [16,18–23]. Both the nonlinearity and the non-normality of the system have been discovered in Rijke tubes [16,20], that the system states can be strongly affected by the initial conditions. For instance, the rapid growth or decay of oscillation can be initiated by either flow or acoustic disturbances even if the disturbances have limited intensity. The flame dynamics in these systems have been studied by the G-equation method, and the flame response to acoustic perturbation has been obtained [24,25]. Some

* Corresponding author.
E-mail address: yz100@sheffield.ac.uk (Y. Zhang).

https://doi.org/10.1016/j.expthermflusci.2023.110923
Received 8 December 2022; Received in revised form 10 March 2023; Accepted 4 April 2023
Available online 8 April 2023

studies have pointed out the importance of the hydrodynamic region around the flame holder in a Rijke tube [19,21]. The nonlinear theoretical model about the hydrodynamic region shows that the system eigenfrequencies and amplitudes can be nonlinearly proportional to system conditions. The hydrodynamic theory indicates the influences of hydrodynamic region position, temperature distribution in tube and geometry properties of the system on generating the self-excited oscillations [19].

The critical roles of several parameters in influencing the thermoacoustic oscillations, including system parameters (e.g. equivalence ratio, fuel flowrate, swirl number) [7,9,10,26,27] and flame dynamics [8,9,28] have been extensively investigated within various combustion systems. It has been found that the equivalence ratio is able to influence many oscillation behaviours, such as frequency response and triggering conditions of beating oscillations [7,18]. The fluctuation of the equivalence ratio has been theoretically proved to be critical for driving the instabilities in a low nitrogen oxide (NOx) gas turbine under lean combustion conditions [29]. The significant effects of fuel flowrate on both amplitude and eigenfrequency of self-excited oscillation in a low swirl burner have been verified [7]. It has been found that both spatial distributions of local equivalence ratio and heat release within the flame area are critical for corresponding thermoacoustic oscillations, also the flame shape is able to influence the relevant oscillation properties [28,30]. Besides, it has been studied that many combustor properties, including fuel injector location, fuel line length, flame location and burner geometry, are effective in characterising stability region, growth factors and states bifurcation in various combustion systems [16,29,31].

Due to the characteristics of nonlinear systems, the system states can be strongly varied with time. Therefore, nonlinear time series analysis methods have been utilised to provide insightful information about system dynamics. Based on trajectory and Poincaré maps constructed from time series measurements in thermoacoustic system, the phase space analysis has been utilised to determine system dynamics, including chaoticity, periodicity and intermittency route to chaos [3,26,31,32]. The Wayland method provides a direct measure of the deterministic nature for a system [33] and it can also be utilised to thermoacoustic systems [26]. This method quantifies the degree of system determinism by calculating the translation error of a state point and its neighbours during the evolution of system [33,34]. In addition, Kaplan-Glass test can also be utilised to quantify the system determinism by coarse-graining the phase space into a grid and evaluating the average directional vectors within it [35,36]. The recurrence plot (RP) is able to provide a direct view of the dynamical properties and the recursiveness of the system [7,27,31,37,38]. Based on the RP, the recurrence quantification analysis (RQA) enables the quantitative descriptions of the system dynamics by obtaining numbers of statistical measures [39]. Therefore, the similarities of systematic dynamics among the different nonlinear systems can be identified, then the system behaviour can be compared among several systems.

Many studies have extensively investigated the effects of different system parameters on the system responses under fuel-lean combustion conditions. However, the fuel-rich combustion condition is preferred for applications which require higher reliability and stableness of combustion, such as Rich-burn, Quick-mix, Lean-burn (RQL) engine. As a reliable system in stationary applications, the rich combustion initiates combustion process in a RQL engine [40]. Meanwhile, the study of nonlinear trends of system responses and the systematic analysis of the different system parameters in a Rijke tube still remains insufficient. Therefore, this study aims to intensively characterise system behaviour and response in a Rijke tube with varied system parameters, including equivalence ratio, fuel flowrate, burner position and tube inner diameter. The pressure fluctuation time series signal has been obtained to analyse system characteristics. The characteristics of the system under different system parameters have been revealed by using multiple time-domain analysis methods. The phase space which is constructed based on the time-delayed embedding method has been applied to qualitatively indicate system nonlinearities. The calculation of Wayland translation error for the trajectory in phase space has been conducted to quantify the system deterministic nature. Both system nonlinear dynamics and recurrence have been investigated by utilising RPs and quantified by the statistical measures from RQA.

2. Methodology

2.1. Experiment setup

The Rijke tube usually consists of a vertically anchored both-open-ended tube and heating elements placed at the lower half of tube [12]. In this study, the experiments were conducted in a Rijke tube with a honeycomb flame holder. The heat source was in the form of a premixed methane-air flame. The schematic figure of the experiment setup is shown in Fig. 1. The quartz tubes (40 and 50 mm in diameters) with a total length of 1 m were utilised as the chamber of the Rijke tube. A honeycomb flame holder with a 22% blockage ratio was applied for stabilising the flame, since the influence of flame holder with this blockage ratio on the thermoacoustic oscillations under the low Mach number conditions can be neglected [41]. During the tests, the burner position was measured from the top of flame holder top to the lower end of tube (z). The Aalborg GFC17 Mass flow controllers were utilised to control flow rates of methane and air, with the accuracy of 0.05% for the methane and 0.1% for the air. The methane flow rate ($\dot{m}_{CH_4}$) was ranged from 0.6 to 1.0 L/min with a step of 0.05 L/min. The equivalence ratios (Φ) at a specific $\dot{m}_{CH_4}$ then could be obtained by the step-changing air flow rates.

A pressure field microphone which was placed at the lower tube end (model PCB 377C10 with a preamplifier PCB 426B03) was utilised to measure time series pressure data. The microphone had a linear frequency response in the range of 10 to 5000 Hz (the practical frequency range of the thermoacoustic system in this study was between 170 and 220 Hz). Besides, the microphone was calibrated by a 10 Pa sinusoidal signal at 1000 Hz before each experiment to ensure conversion accuracy for the collected pressure fluctuation signal. The signal was sampled at a sampling rate of 100,000 Hz for 10 s to ensure the accuracy of frequency analysis results. The time series pressure fluctuation data was acquired by the NI-9205 Voltage input module with the Chassis cDAQ-9178. Two

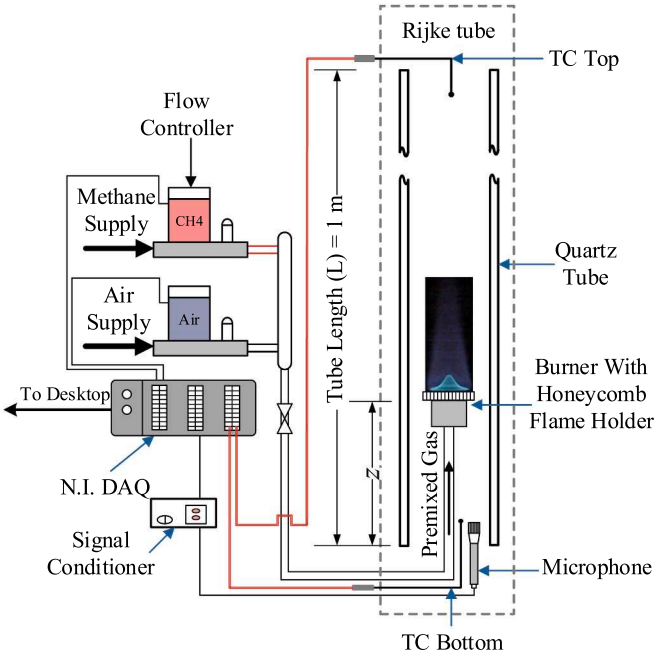

Fig. 1. Schematic figure of the flame-driven Rijke tube.

RS type-N thermocouples (TC) were used to measure the temperature at both upper and lower ends of tube. The accuracy of thermocouples was ± 1.5 K. The measured temperature data was acquired by the NI-9211 Temperature Input Module at a sampling rate of 10 samples per second. A stabilisation time of 3 min for the system was processed to ensure that the system had exited the transition process and the stableness of system states.

2.2. Data processing method

2.2.1. Phase space analysis

In this study, the 3-dimensional phase space was reconstructed to investigate the oscillation properties in the time-domain. The trajectory in the phase space was obtained based on the time series data of the pressure fluctuations. Based on the Takens' time-delay embedding theorem [42], the vector in the phase space, which was formed by the pressure time series data, can be expressed in the following form:

$$\mathbf{P}'_{t}(\mathrm{D}) = (p'(t), p'(t-\tau), p'(t-2\tau), \cdots, p'(t-(D-1)\tau)) \quad (1)$$

where the $\mathbf{P}'_{t}(D)$ represents the vector in phase space with an embedding dimension of D, $p'(t)$ denotes the normalised time series pressure fluctuations data at time t, τ denotes the time delay. In order to compare the trajectories with different oscillation amplitude, the pressure time series was normalised ($p^*(t)$) based on its maximum absolute value, as $p^*(t) = p'(t)/(\max(|p'(t)|)$. The time delay is critical for forming phase space trajectory by the time-delay method. The inappropriate time delay values could lead to the incorrect correlation between the points and the trajectory, making it unable to indicate the correct characteristics of oscillations [26]. The autocorrelation function and average mutual information are suggested to determine the value of time delay [3,26]. In this study, the time delay was determined by the first zero-crossing point of the autocorrelation functions since the self-excited oscillation was periodic with low complexity and chaoticity, neither no intermittency nor chaos states were found. The Wayland translation error (e_{trans}) was utilised to further recognise the system stability by quantifying system deterministic nature. The algorithm is proposed by Wayland et al [33], and it is applicable to the time delay vector from the time series data [26,34]. Wayland method quantifies the system deterministic natures by calculating the errors of translation for a specific state point and its nearest k-neighbours to their images through the translation vector between the original and image point. The images of this state point and it its nearest k-neighbours is obtained by mapping the original points with a certain time interval. For a fully deterministic system, the translation vectors are same, meaning that no translation error. For the space vector obtained from time-delayed embedding method, the translation vectors ($\mathbf{v}_{\mathrm{trans}}$) will be in the following form:

$$\mathbf{v}_{\mathrm{trans}}(\mathrm{t_k}) = \mathbf{P}'_{\mathrm{t_k+m}} - \mathbf{P}'_{\mathrm{t_k}}, \mathbf{P}'_{\mathrm{t_k}} \in \{\mathbf{V}\}^K \quad (2)$$

where subscript m denotes the specific time interval for the determination of translation vectors, of which the value is suggested to be the same value as τ [34]. $\{\mathbf{V}\}^K$ is the series of neighbour vectors with the amount of K to the randomly selected $\mathbf{P}'_{\mathrm{t_0}}$. The subscript k represents the k-th nearest neighbour vectors to $\mathbf{P}'_{\mathrm{t_0}}$. In this study, K was set to 100 to provide the reliable result on $\overline{\mathbf{v}}(\mathrm{t})$. The vectors in $\{\mathbf{V}\}$ are in the nearest order, which is determined based on the Euclidean metric between the $\mathbf{P}'_{\mathrm{t_k}}$ and $\mathbf{P}'_{\mathrm{t_0}}$. The nearest neighbour should satisfy $|\mathrm{t_k} - \mathrm{t_0}| \rangle \tau$ to avoid the temporal correlation [33,34]. The average translation vectors $\overline{\mathbf{v}}(\mathrm{t_k})$ then can be defined as below:

$$\overline{\mathbf{v}}(\mathrm{t}) = \frac{1}{K+1}\sum_{k=0}^{K}\mathbf{v}_{\mathrm{trans}}(\mathrm{t_k}) \quad (3)$$

Then, e_{trans} can be calculated based on the following equation:

$$e_{trans} = \frac{1}{K+1}\sum_{k=0}^{K}\frac{\|\mathbf{v}_{\mathrm{trans}}(\mathrm{t_k}) - \overline{\mathbf{v}}(\mathrm{t})\|^2}{\|\overline{\mathbf{v}}(\mathrm{t})\|^2} \quad (4)$$

In this study, in order to provide a better statistical result, the median e_{trans} was obtained by randomly selecting 10 different $\{\mathbf{V}\}$ and calculating the corresponding e_{trans}. K was set as 100 to provide reliable results of $\overline{\mathbf{v}}(\mathrm{t})$ and e_{trans}. The value of e_{trans} could provide quantitative measures of system deterministic nature. Generally, smaller e_{trans} indicates more deterministic system, while higher e_{trans} for more chaotic and complex system. For a system with an ideally random nature, the value of e_{trans} would be 1, while the criterion value of e_{trans} for a deterministic system would be 0.01 [26].

2.2.2. Recurrence analysis

The state recursiveness in a dynamical system is usually considered as a key characteristic to describe the system behaviour in a system with high complexity, such as the combustion instability in a combustion system [7,43,44]. Therefore, the recurrence analysis could effectively determine the system dynamics of self-excited thermoacoustic oscillations in a Rijke tube [3,7]. Recurrence Plot enables the visualisation of states recurrence by obtaining recurrence matrix $\mathbf{R}$. $\mathbf{R}$ is a binary matrix as below:

$$\mathbf{R}_{\mathrm{i,j}} = \Theta\left(\varepsilon - \|\boldsymbol{x}_i - \boldsymbol{x}_j\|\right) i, j = 1, 2, 3, \cdots, N \quad (5)$$

where $\boldsymbol{x}$ denotes the space vector obtained from the discrete time series data $X(t)$ according to the time-delayed embedding method, as shown in Eq. (1). Subscripts i and j are sequence of space vectors and coordinates. $\|\boldsymbol{x}_i - \boldsymbol{x}_j\|$ denotes the norm of difference between $\boldsymbol{x}_i$ and $\boldsymbol{x}_j$. Θ is the Heaviside function. ε is the recurrence threshold to determine whether two target points can be considered recurrent. The selection of ε is critical in recurrence analysis since the improper ε may lead to dramatic changes in results or an unfaithful result [36,45,46]. A criterion that ε should not exceed 10% of the mean phase space diameter has been proposed by Schinkel et al. and Marwan et al. [35,43]. Meanwhile, it is also suggested that the standard deviation can be taken into account for the captured noisy discrete signal [39]. In this study, the ε was set as 15% of the standard deviation (σ) of the corresponding pressure fluctuation time series signal, which was suggested by Zan et al. [47]. This ε also satisfied the criterion of mean phase space diameter. Therefore, the ε was varied with cases and depending on the corresponding attractor size of each case. Another critical parameter for obtaining $\mathbf{R}$ is the embedding dimension since the recurrence analysis is based on the results of lag-reconstructed from time series signal [7,44]. A proper selection of embedding dimension should be able to avoid spurious correlations and minimise the presence of orthogonal diagonal lines to line of identity (LOI, $\mathbf{R}_{\mathrm{i,i}} = 1$). The proper embedding dimension for recurrence analysis (D_{rec}) can be obtained by false nearest neighbours (FNN) method. In this study, D_{rec} was set to 3 according to the FNN method. The time delay for recurrence analysis (τ_{rec}) was also determined based on first zero-crossing point of autocorrelation functions. For a periodic system with a smooth phase space, a high sampling rate will result in spurious quantifications, and the RP consists of large amounts of exclusively diagonal line structures. Due to this, a very high value of determinism (DET) can be resulted into, which leads to the situation that characteristics of the periodic system cannot be clearly and sufficiently indicated [48,49]. It has been suggested that 8 to 10 sampling points should be included within each period [37]. In this study, a down-sampling process was conducted to meet the requirements of 10 sampling points per period by selecting 10 space vectors with a constant time interval for each period. Therefore, the high accuracy of results and clear indications of state changes can be achieved.

Based on the structural properties of the RP, the Recurrence Quantification Analysis (RQA) can further quantify system dynamics. In this study, four measures, including recurrence rates (RR), determinism

(DET), Shannon Entropy (ENT) and average diagonal line length (ADL), were used to indicate various system nonlinear dynamics, including both periodicity and complexity [38,39,44]. These measures can be expressed in the following forms:

$$\mathrm{RR}(\varepsilon) = \frac{1}{N^2}\sum_{i,j=1}^{N}\mathbf{R}_{i,j}(\varepsilon) \tag{6}$$

$$\mathrm{DET} = \frac{\sum_{l=l_{min}}^{N} lP(l)}{\sum_{l=1}^{N} lP(l)} \tag{7}$$

$$\mathrm{ADL} = \frac{\sum_{l=l_{min}}^{N} lP(l)}{\sum_{l=min}^{N} P(l)} \tag{8}$$

$$\mathrm{ENT} = -\sum_{l=l_{min}}^{N} p(l)\ln p(l) \tag{9}$$

where N denotes data length for recurrence analysis which is obtained from time series signal based on embedding dimensions. The density of recurrence points in the RP can be determined by RR. DET is defined as the ratio of recurrence points which forming the line structure in the diagonal direction to all recurrence points. $P(l)$ represents histogram of the diagonal lines with length of l. l_{min} denotes the least length of diagonal, and the value in this study was set to 2. The occurrence of similar states then can be determined by DET. The average diagonal line length (ADL) is able to obtain the average time that two segments in the trajectory are close to each other, and the degree of parallelism. The ENT is able to determine Shannon Entropy based on the entropy of $p(l)$. $p(l)$ represents the probability of appearance for the diagonal line with a length of exactly l. $p(l)$ is obtained by $p(l) = P(l)/N_l$, where N_l denotes the number of diagonal lines. The system complexity and chaoticity then can be indicated by ENT. The Shannon Entropy in this study was calculated based on the natural logarithm with the unit of *nat*.

3. Result and discussion

Thermoacoustic oscillations are usually involved with the interactions between heat release and pressure fluctuation. Therefore, the system parameters, including fuel flowrate ($\dot{m}_{CH_4}$), equivalence ratio (Φ), burner position (z) and tube inner diameter (ID), are able to strongly influence oscillation behaviours. In this study, the effects of these system parameters on both system frequency response and systematic characteristics are focused on. Based on experimental results, multiple system analyses, including frequency analysis, phase space and corresponding translation error, and recurrence analysis, are conducted to reveal the frequency response, deterministic natures and nonlinear dynamics of thermoacoustic systems under different system parameters.

3.1. System frequency response and oscillation amplitude

The results of eigenfrequency (f_{eigen}) and root mean square acoustic pressure (P_{rms}) for the case at L/4 and L/12 of burner positions with varied methane flowrates are shown in Fig. 2. The f_{eigen} is the dominant eigenfrequency of the self-excited thermoacoustic oscillation, which is obtained from the frequency spectrum of the oscillation. It is found that the eigenfrequencies of these cases are the fundamental harmonic mode due to its greater intensity than higher harmonic modes. For 40 mm cases, by comparing the results at the same burner position, it can be found that the eigenfrequency presents similar nonlinear trends along various equivalence ratios under the same $\dot{m}_{CH_4}$, as shown in Fig. 2 (a) and (b). In detail, a certain Φ-sensitive range ($1.3 < \Phi < 2$) and an Φ-insensitive range ($\Phi > 2$) of f_{eigen} can be obtained from the Fig. 2. In Φ-sensitive range, it is found that f_{eigen} is sensitive to the change of Φ, and a decreasing trend of f_{eigen} with increasing Φ can be observed in most cases. Be different from the Φ-sensitive range, the f_{eigen} becomes insensitive to Φ changes and the f_{eigen} becomes nearly constant once Φ becomes greater than 2. The nonlinear trends between f_{eigen} and Φ might be caused by the changing rate of net heat release to Φ in the range of

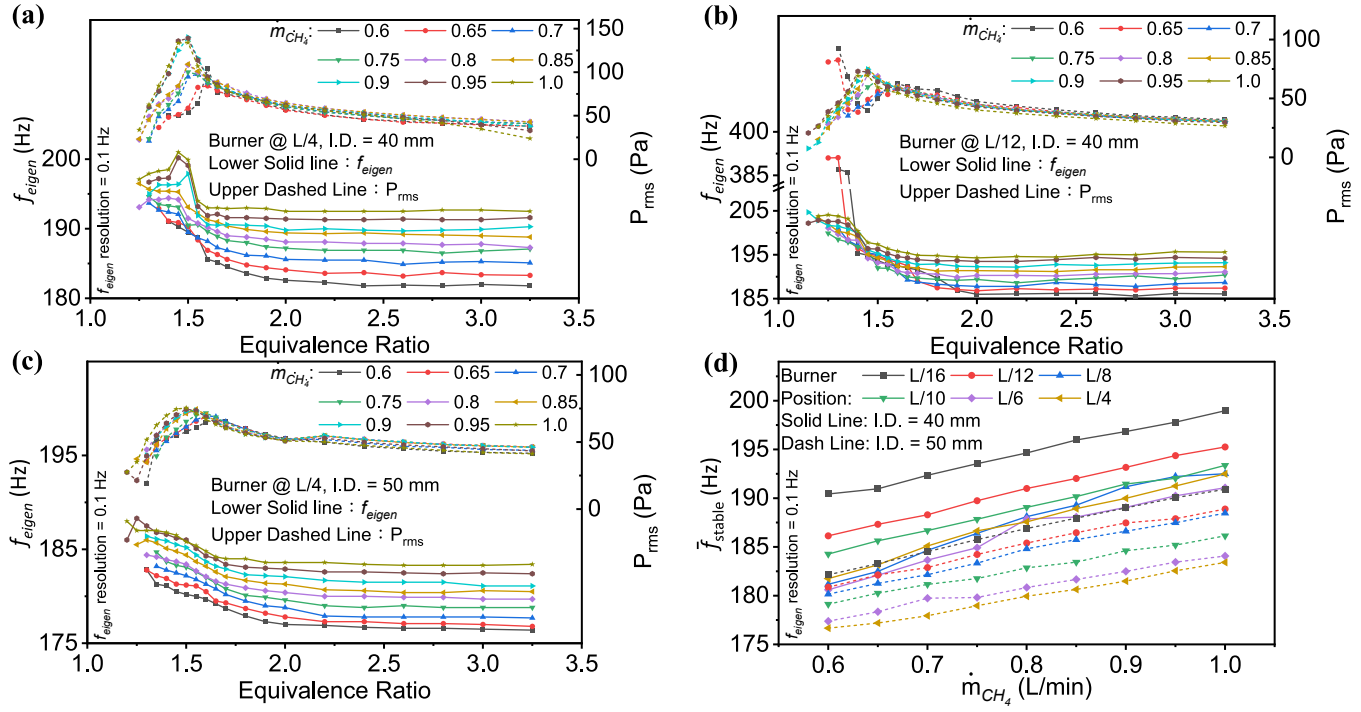

Fig. 2. System dominant eigenfrequency (f_{eigen}) and root mean square acoustic pressure (P_{rms}) at various Φ ($\dot{m}_{CH_4}$ ranged from 0.6 to 1.0 L/min) under the conditions: (a): ID = 40 mm, burner position of L/4; (b): ID = 40 mm, burner position of L/12; (c): ID = 50 mm, burner position of L/4. The corresponding f_{eigen} and P_{rms} are represented by solid lines and dashed lines respectively in figure (a) to (c). Figure (d) represents the $\bar{f}_{stable}$ changes to the $\dot{m}_{CH_4}$ at various burner positions, where the solid and dashed lines denote 40 and 50 mm, respectively.

$\Phi > 2$. It has been reported that the net heat release of premixed methane flame in fuel-rich range is inversely proportional to increasing Φ when the methane flowrate keeps constant, and the decreasing rate of net heat release decreases with increasing Φ, especially when Φ is greater than 2 [18]. This trend is also possibly arising from the changes in flame length. It is found that the trend of system eigenfrequency is related to the trend of visible flame length (L_{flame}) when the methane flowrate keeps constant, as shown in Fig. 3 (a). The L_{flame} exhibits a general increasing trend followed by a less varied but still slightly increasing trends as Φ increases. In this study, the change in Φ is obtained by maintaining a constant methane flowrate, thereby leading to the total heat power remaining approximately constant. Since the occurrence of secondary combustion, which results from fresh air supply through the convective flow drawn from the bottom end, keeps consuming the incompletely reacted species at a higher Φ. Thus, a longer flame length under a higher Φ can lead to a smaller heat release per unit area. Combined with the lower adiabatic flame temperature at a higher Φ, this can lead to a smaller temperature gradient in the downstream region. As Φ exceeds 2, the flame length tends to stabilise with less variation. The general flame temperature also becomes generally stable due to the more important role of diffusion effect in the flame under higher Φ, which is evidenced by the inapparent inner cone layer and the occurrence of soot, as shown in Fig. 3 (b). In addition, it was found in the previous study that the characteristics of change in time-evolution of pressure fluctuations and the system dynamical properties presented the same nonlinear trend to Φ, which indicates the existence of Φ-dependence and independence ranges of system response [50].

An increasing-then-decreasing trend of P_{rms} is found among all cases, of which the turning point is defined as where the trend of P_{rms} changes. P_{rms} presents an increasing trend as Φ increases before Φ reaches the maximum value, indicating the increases in Rayleigh Index and the more favourable phase between heat release and pressure fluctuation. For a specific premixed laminar flame, its heat release is proportional to its flame surface area and variation of flame front [51,52]. In addition, the maximum heat release of a premixed flame is obtained at its rapid reaction region [53,54]. Fig. 3 (b) shows the example flame photos under different Φ while keeping the methane flowrate the same. In this case, the turning point of P_{rms} was 1.7. It can be seen that the luminous inner cone layer of the flame, which is formed by the rapid reaction region due to the chemiluminescence, is more obvious when $\Phi < 1.7$, indicating significantly strong local heat release at this position compared to its downstream equilibrium region [55]. However, the cases that $\Phi > 1.7$ present a less obvious inner cone layer, which is caused by the thickening of the reaction region due to the stronger diffusion effect of fuel, lower reaction rate, and lower flame temperature at a higher Φ [55,56]. The inapparent inner cone also indicates less heat release gradient along the flame. Meanwhile, the pressure fluctuations modulate the flame and result in the stretching and wrinkling from its bottom position, which is more closely to the rapid reaction region. Under this circumstance, the rapid reaction region can be more easily disturbed by pressure perturbations, leading to the modulation of heat release. Whereas, the inapparent rapid reaction region of the flame at a higher Φ indicates a thicker reaction region and a more uniform distribution of heat release within the flame, implying less modulation of heat release by the pressure perturbations. Thus, the heat release of the flame with a higher Φ ($\Phi > 1.7$) shows less sensitivity to the modulation effect of pressure fluctuations than the flame with a lower Φ ($\Phi < 1.7$). In addition, the inner cone layer becomes even more inapparent as Φ keeps increasing, resulting in the fluctuation of flame heat release being furtherly less modulated by the pressure fluctuations. This leads to a decreasing Rayleigh index and less intense oscillation as Φ increases when $\Phi > 1.7$, and a decreasing trend of P_{rms} is obtained in this Φ region.

As Φ increases from 1.4 to 1.7, it can be found that the reaction region gradually detaches from the flame holder, which means it is more easily affected by the pressure fluctuations. The inner cone layer is stretched and disturbed by pressure fluctuations, leading to the deformation and wrinkle of this cone layer and the change in the surface area of this layer. Considering that the modulation effect of pressure fluctuations initiates from the root of the flame, which is closer to the reaction region, the fluctuation of heat release becomes to be more modulated by the pressure fluctuations as Φ increases from 1.4 to 1.7, resulting in an increasing trend of P_{rms} in this Φ region. In addition, it has been found that both deformation and oscillation of flame (including flame suppression and stretch) due to acoustic wave can result in the inhomogeneity of local Φ and the local heat release rate in flame if the fuel and air supply are initially separated [29]. Considering the flame is relatively shorter in the range $1.4 < \Phi < 1.7$, as shown in Fig. 3 (b), a greater gradient of local Φ within the flame can be achieved. Due to the influences from the local heat release rate and Φ, the heat release rate fluctuations can be strongly affected and driven by the self-excited pressure oscillation. Thus, the heat release rate fluctuations may become more in-phase with pressure fluctuations, which implies an increasing Rayleigh index [11,14]. As a result, the effect of excitation becomes more intense and leads to a greater oscillation amplitude. In addition to this, it is also found that the turning point of P_{rms} is slightly prior to the turning point of Φ, that P_{rms} is earlier became less sensitive to Φ than f_{eigen}. It implies the critical roles of Φ in characterising self-excited thermoacoustic oscillations that the system response can be nonlinearly related to Φ. It may also indicate the system response delay between amplitude and frequency.

By comparing the curves of f_{eigen} at different $\dot{m}_{CH_4}$, the importance of fuel flowrate in characterising oscillations can be highlighted. It can be seen that the systems with a higher $\dot{m}_{CH_4}$ generate higher f_{eigen} regardless of burner position change, especially in the Φ-insensitive range. In order to further analyse the system frequency response with varied $\dot{m}_{CH_4}$ in the Φ-insensitive range, the mean stable eigenfrequency ($\bar{f}_{stable}$) is obtained

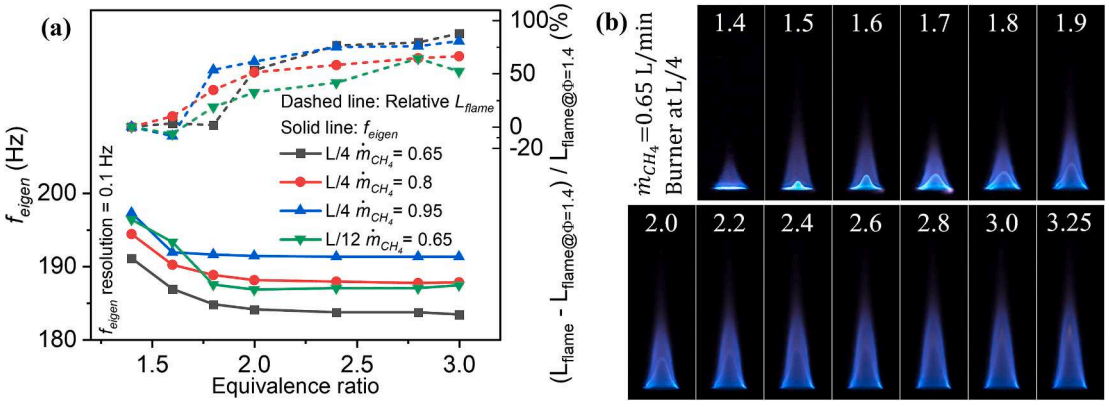

Fig. 3. (a)f_{eigen} and relative L_{flame} (calculated based on L_{flame} at $\Phi = 1.4$, as $(L_{flame} - L_{flame@\Phi=1.4})/L_{flame@\Phi=1.4}$) to Φ, and (b) examples of flame photos.

by calculating the mean value of f_{eigen} in the Φ-insensitive range (Φ > 2). The curves of $\bar{f}_{stable}$ to $\dot{m}_{CH_4}$ are plotted in Fig. 2 (d). It can be found that $\bar{f}_{stable}$ presents an approximately linear relationship with increasing $\dot{m}_{CH_4}$. Similar gradients of $\bar{f}_{stable}$ trending lines with varied $\dot{m}_{CH_4}$ can be observed from the cases at different burner positions or ID. Overall, considering the situation of larger fuel flowrate, the eigenfrequency increase might be caused by higher total heat release and higher mean temperatures [7]. However, the P_{rms} presents very small differences with varied fuel flowrates after the turning points. From the cases of 50 mm ID, the nonlinear trends between f_{eigen} and Φ can be also obtained, also the influence of $\dot{m}_{CH_4}$ on both f_{eigen} and P_{rms} are illustrated (e.g. Fig. 2 (c)). Besides, the linear relationship between $\dot{m}_{CH_4}$ and $\bar{f}_{stable}$ at different burner positions are obtained (e.g. Fig. 2(d)).

Fig. 3 presents the corresponding system eigenfrequency under various equivalence ratios at different burner positions. It can be seen that f_{eigen} is obviously affected by burner position in the whole Φ range, as shown in Fig. 4. Approximate 10 Hz of $\bar{f}_{stable}$ change under the same $\dot{m}_{CH_4}$ and ID can be obtained when moving the burner from L/4 to L/16. Focusing on the changes of $\bar{f}_{stable}$ to burner position, the cases of 40 mm present non-monotonical trends of $\bar{f}_{stable}$ with increasing burner position can be obtained, as shown in Fig. 4 (d). Such non-monotonical trends are likely caused by the hydrodynamic region around the flame holder, since similar trends have been theoretically and experimentally discovered by Heckl and Zhao in the Rijke tube [19,21]. However, it is found that the trends are monotonically decreasing in the cases of 50 mm ID. The reason for the monotonical trends in the 50 mm tube might be the less influence from the hydrodynamics region due to the larger ID. It is also found that the burner position is vital to the changes of dominant mode, as the harmonic modes shifting of eigenfrequencies can be found in some cases, as highlighted in Fig. 2 (b), Fig. 4 (a) and (c). The second harmonic mode can be the dominant mode (the intensity of the fundamental mode is neglectable) when Φ is closer to 1 and the burner is at lower positions, such as L/16 and L/12. Considering the longer region after flame when the burner is moved downward, both effective length and acoustic reflection boundary are changed, which may further lead to the change of instability trait of flame [27]. Meanwhile, higher heat power also leads to changes in oscillation modes [23]. Thus, the shift of the dominant harmonic mode can be triggered under such circumstances. For the oscillation amplitude, the important role of burner position also can be discovered from the high dependency of P_{rms} on burner position at a low $\dot{m}_{CH_4}$, as shown in Fig. 4 (a) (c). From the Fig. 4 (d), it is found that the increasing rates of $\bar{f}_{stable}$ to $\dot{m}_{CH_4}$ at different burner positions are similar, which means those trends are regardless of burner position change. Meanwhile, similar gradients of $\bar{f}_{stable}$ change with increasing $\dot{m}_{CH_4}$ are found from both 40 and 50 mm cases. Therefore, it can be concluded that the linear relationships between $\dot{m}_{CH_4}$ and $\bar{f}_{stable}$ are independent with both burner position and tube ID.

Besides, it can be found that increasing ID can lead to decreasing eigenfrequency, as shown in Fig. 2 and Fig. 4. For this decreasing trend, it can be caused by the decreased mean sound speed in the tube due to lower mean temperature in the downstream region in 50 mm tube. Since the input heat remains constant (the heating source remains the same), the mean temperature of the downstream flow is heated into a lower value due to the larger corresponding volume caused by a larger ID. In order to validate this, a simplified model is developed in this study. The tube can be generally divided into two regions based on the temperature. The region after flame (downstream, represented by subscript u) is the high temperature region, while the region before flame is low temperature region (upstream, represented by subscript d). Compared to the total length of tube, the flame length is relatively short. Thus, it can be assumed that the effects of acoustic characteristics inside the flame are neglected since the less influence by sound speed changes inside the flame. Note that it is assumed that gases at both upstream and downstream regions are homogenous. Considering the sound speed difference due to temperature difference at both regions, the average sound speed, c_{avg}, along the tube can be expressed as:

$$c_{avg} = \frac{L}{t_a} = \frac{L}{\frac{l_u}{c_u} + \frac{l_d}{c_d}} \tag{10}$$

where L is the length of the organ pipe and t_a is the travelling time of acoustic wave. Respectively, l_u and l_d represent the length of upstream and downstream region. Considering that the heating effect of the flame is mainly in axial direction of fuel jet rather than the radial direction, the temperature near the flame in the radial direction would be relatively lower compared to the temperature in the axial direction after the flame.

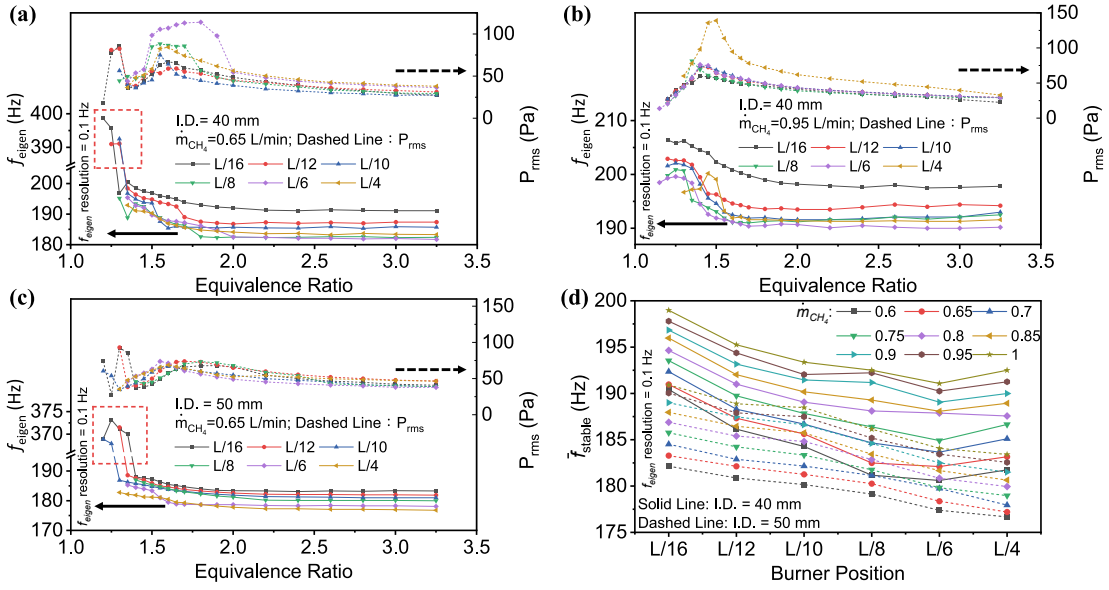

Fig. 4. System dominant eigenfrequency (f_{eigen}) and P_{rms} to various Φ at burner positions from L/4 to L/16 in the system under the condition: (a): ID = 40 mm, $\dot{m}_{CH_4}$ = 0.65 L/min; (b): ID = 40 mm, $\dot{m}_{CH_4}$ = 0.95 L/min; (c): ID = 50 mm, $\dot{m}_{CH_4}$ = 0.65 L/min. The corresponding f_{eigen} and P_{rms} are represented by solid lines and dashed lines respectively in figure (a) to (c). Figure (d) represents the $\bar{f}_{stable}$ changes to the burner positions at various methane flowrates, where the solid and dashed line denote the 40 mm and 50 mm, respectively.

Besides, the fuel-rich premixed conical laminar methane flames in this study have a hollow structure, that the inner cone of the flame is filled with unburnt premixed gas at a relatively low mean temperature compared to the downstream of the flame. Thus, the flame region is considered to be the low temperature region. Then, η can be determined by the ratio of the sum of the burner position and flame length to the tube length. Based on η, l_u and l_d can be expressed as:

$$l_u = \eta L, l_d = (1-\eta)L \tag{11}$$

Assuming the gas in the tube is ideal, and substituting the l_u, l_d into Eq. (10), the expression for c_{avg} based on ideal gas law, then can be given as:

$$c_{avg} = \frac{\sqrt{\gamma_u T_u \gamma_d T_d R}}{(1-\eta)\sqrt{\gamma_u T_u} + \eta\sqrt{\gamma_d T_d}} \tag{12}$$

where γ is the adiabatic index, the value is determined based on measured temperature T. R denotes the gas constant. The frequency of a standing wave in an organ pipe with the consideration of end corrections (e) can be calculated by the following equation:

$$f = \frac{nc}{2(L+e)} \tag{13}$$

where n represents the mode number. In this analysis, $n = 1$ for the fundamental mode. The end correction in this study is determined by $e = 0.6$*ID. Therefore, substituting Eq. (12) into Eq. (13), the ratio between the frequency in the tube with ID of 40 mm (f_{40}) to 50 mm (f_{50}) can be expressed as:

$$r_{40/50} = \frac{f_{40}}{f_{50}} = \frac{\left(\frac{\sqrt{\gamma_u T_u \gamma_d T_d}}{(1-\eta)\sqrt{\gamma_u T_u}+\eta\sqrt{\gamma_d T_d}}\right)_{40mm}}{\left(\frac{\sqrt{\gamma_u T_u \gamma_d T_d}}{(1-\eta)\sqrt{\gamma_u T_u}+\eta\sqrt{\gamma_d T_d}}\right)_{50mm}} \times \frac{(L+e_{50})}{(L+e_{40})} \tag{14}$$

Based on measured T_u and T_d, the results of $r_{40/50}$ are shown in Fig. 5. It can be seen that the results from the modelling prediction are in good agreement with the experimental results. The analysis results prove the important roles of average sound speed and mean temperature inside the tube in characterising the frequency response of the Rijke tube.

The results of system response in both eigenfrequencies and oscillation amplitudes have shown that the system could be generally divided into two ranges based on the sensitivity to Φ. The system appears to be similar in such ranges among all cases. Therefore, for ease of comparison, Φ = 1.4 and 3.0 are specially selected for further analysis and comparisons in most cases.

3.2. System properties from phase space

The 3-dimensional phase space of pressure fluctuations is reconstructed based on the time-delayed embedding phase space vector [42], $\mathbf{P}'_t(3) = (p^*(t), p^*(t-\tau), p^*(t-2\tau))$. The time series data of pressure fluctuations $p'(t)$ are normalised based on the maximum value of corresponding time series, thus the trajectories of the oscillations with different amplitudes become comparable. The results of 3-dimensional phase space are shown in Fig. 6. It can be seen that the trajectories of periodic oscillation are clearly formed in all cases, and the differences in the 'width' of trajectory can be clearly observed as well. For the trajectory with a 'thinner' width, the system is more periodic and stable. At the burner positions of L/4, a single-loop trajectory can be observed in all cases, which implies the period-1 oscillation under such conditions. Meanwhile, it also indicates that the oscillation is characterised by a single frequency [57]. The trajectories for the cases at Φ = 1.4 present the 'widest' trajectory regardless of the changes of $\dot{m}_{CH_4}$ when the burner is at L/4. At the same $\dot{m}_{CH_4}$, the 'thinner' trajectories at increased Φ indicate the oscillations with more limit-cycle characteristics. The trajectory 'width' change indicates a more stable and less complex oscillation as the combustion condition becomes richer when the burner is placed at higher burner positions. For the system in the Φ-insensitive range (Φ = 3.0), the changes of $\dot{m}_{CH_4}$ show less influence on the properties of oscillations since the trajectories present barely noticeable change with increasing $\dot{m}_{CH_4}$. While the stableness of the system slightly varies with the increasing $\dot{m}_{CH_4}$ when Φ = 1.4 at the same burner position. However, as the burner is moved lower to L/16, the trajectory become more complex and 'wider' as Φ increases, as shown in Fig. 6 (d) and (h). The beating oscillation is triggered for the cases at Φ = 3.0 and L/16 of burner position. It can be found that the trajectories of Φ = 3.0 are obviously wider and more complex than Φ = 1.4 cases. Both the trajectories of are 2-tori in the phase space, which implies that oscillations have two incommensurate frequencies [57]. Such properties indicate the quasi-periodic oscillations at Φ = 3.0 and L/16 of burner position. Besides, the oscillations in fuel-rich combustion conditions show lower complexity and stability at a higher burner position (L/4) compared to the cases at a lower burner position (L/16).

In order to further determine the characteristics of system from the results of phase space analysis, the Wayland method is conducted to obtain the e_{trans} of trajectory, as shown in Fig. 7 and Fig. 8. The e_{trans} slightly increases with the increasing embedding dimensions when the embedding dimension is greater than 3 in most cases. It indicates more parallelism of neighbouring trajectories at lower embedding dimensions in this system [26]. The values of the median e_{trans} of self-excited oscillations are smaller than the gaussian white noise (about 1) and the criterion value for the deterministic system (0.01), as the order of magnitude is about 10^{-5} to 10^{-2}. This implies that the triggered oscillations can be considered to be periodic oscillations, and the systems have sufficient deterministic natures. In the cases at ID of 40 mm, it is found that the e_{trans} can be affected by the combustion related parameters since its values range from 10^{-5} to 10^{-4}, as shown in Fig. 7. By comparing the cases with the same $\dot{m}_{CH_4}$ as shown in Fig. 7 (a), it can be observed that the e_{trans} trends to decrease with the increasing Φ, which indicates the more periodic and less complex oscillation at a higher Φ. While slight changes can be still observed from some cases with increased Φ even in the Φ-insensitive range. The effective role of Φ in the

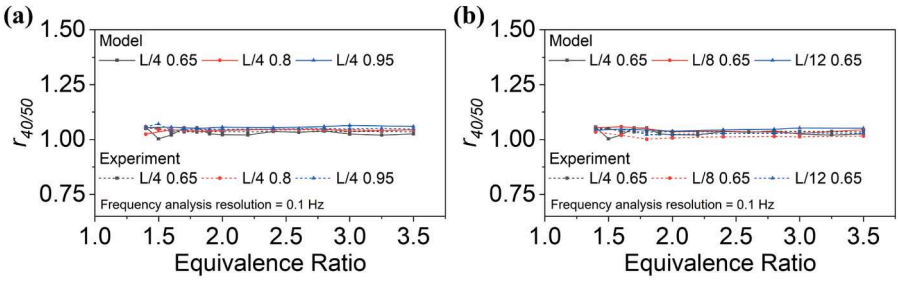

Fig. 5. Ratios of eigenfrequencies in ID 40 mm to 50 mm tube with the varied equivalence ratios under (a): $\dot{m}_{CH_4}$, and (b): burner positions. The legend is in the form of: {Burner position, $\dot{m}_{CH_4}$}. The solid lines represent the experimental data of the eigenfrequency ratio, and the dashed lines represent the modelling prediction result based on measured temperatures at both ends of the tube.

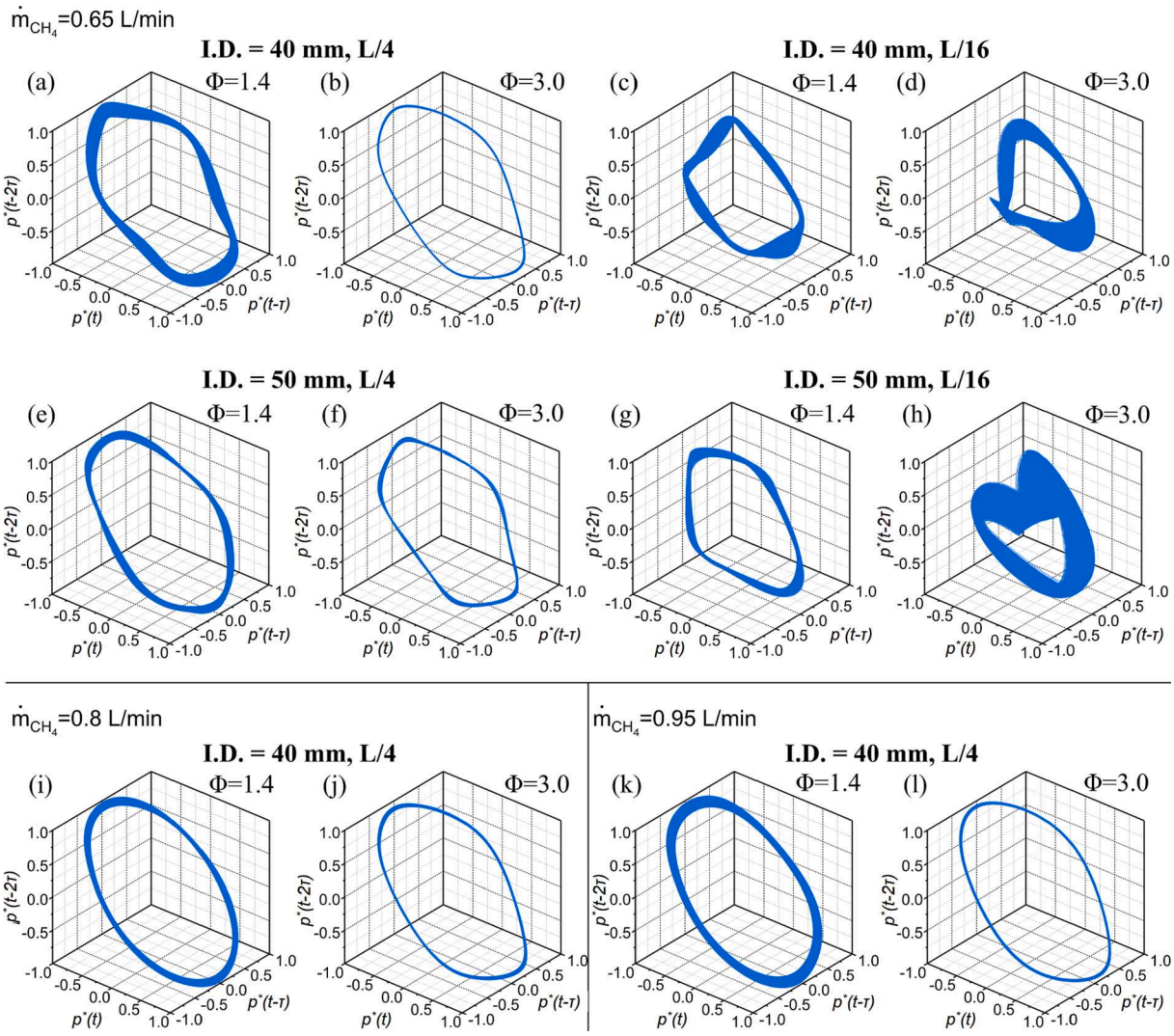

Fig. 6. The trajectories of the normalised time series data $(p^*(t), p^*(t-\tau), p^*(t-2\tau))$ which are constructed from the space vectors in the 3-Dimensional phase space under difference equivalence ratios, fuel flowrate, burner position of L/4 and L/16, and ID of 40 mm and 50 mm. ((a)~(h): the $\dot{m}_{CH_4} = 0.65L/min$; (e), (f): $\dot{m}_{CH_4} = 0.80L/min$; (g), (h): $\dot{m}_{CH_4} = 0.95L/min$. The corresponding equivalence ratios are shown at the top-right corner of each figure, and the burner positions and ID of the tube are shown on the top of the set of figures.).

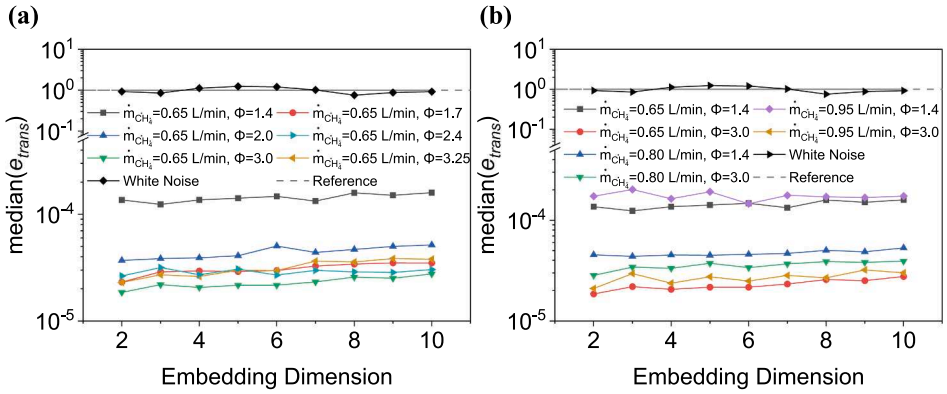

Fig. 7. Median translation error ($median(e_{trans})$) to embedding dimension for the time series data of pressure fluctuation at (a) different Φ and Gaussian white noise, with the K = 100. The dashed line at$e_{trans} = 1$ represents the ideally random process.

system deterministic nature can be highlighted, since the fluctuation of e_{trans} shows that the system states are still slightly varying with Φ, as shown in Fig. 7. Meanwhile, it also shows that the Wayland method is more effective to reveal the properties of the system, as the frequency response is relatively stable in the Φ-insensitive range, as shown in Fig. 2. Considering the special properties of the cases at Φ = 1.4 and 3.0

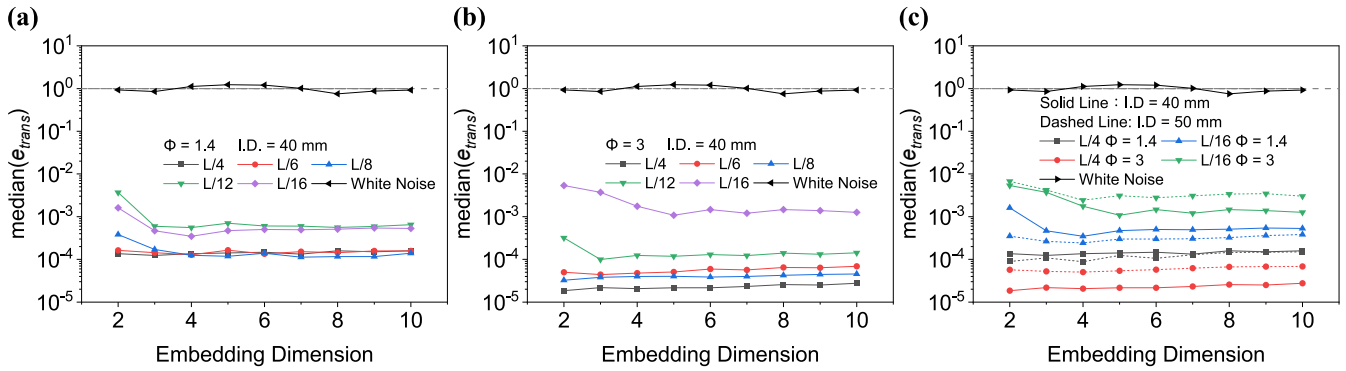

Fig. 8. The *median*(e_{trans}) to embedding dimension under different burner positions for the cases with different Φ of (a) Φ = 1.4 and (b) Φ = 3 but the same $\dot{m}_{CH_4}$ of 0.65 L/min. (c) Comparisons between the system with different IDs. K = 100. The dashed line ate_{trans} = 1 represents the ideally random process.

as discussed above, they are selected to represent the system deterministic natures. Compared to the cases of Φ = 3.0, it can be found that the $\dot{m}_{CH_4}$ is more efficiently influencing the e_{trans} when Φ = 1.4. The e_{trans} of the cases at Φ = 1.4 strongly vary with the increasing $\dot{m}_{CH_4}$ as shown in Fig. 7 (b). In contrast, the e_{trans} for the cases of Φ = 3.0 have similar values with each other without significant difference, and the values are smaller than the cases of Φ = 1.4. Therefore, the deterministic nature of the system can be more likely affected by $\dot{m}_{CH_4}$ if the system is in the Φ-sensitive range (conditions as lower Φ).

From Fig. 8, it can be seen that the e_{trans} appears to be more variant with burner position changes, as its values are in larger ranges of 10^{-5} to 10^{-2}. Thus, the burner position can be more effective in influencing system stability and deterministic nature compared to Φ and $\dot{m}_{CH_4}$. Meanwhile, the e_{trans} tends to be more affected by the burner position changes as the burner moves to a lower position. The e_{trans} is found to be higher at a lower burner position (L/12 and L/16) in conditions of Φ = 1.4 and 3.0. The higher value of e_{trans} implies that the system becomes less deterministic and more complex when the burner approaches the lower tube end. It is possibly caused by more complex flow conditions around the flame at the position closer to the tube end. The nonlinear oscillation can be more easily affected by external disturbance under this condition, as the effect of flow around the flame has been found to be vital to the oscillation stability [23]. Under such circumstances, it seems that a lower overall supply flowrate and amount of heat release might increase the sensitivity of the system to flow disturbance around the flame. The cases with higher Φ but the same $\dot{m}_{CH_4}$ can be the examples of the case with lower overall flowrate and heat release. Because the net heat release of the premixed methane flame has been found to be inversely proportional decreasing with the increasing Φ under the same $\dot{m}_{CH_4}$, if Φ is in the investigated range of this study [18,52]. From the experimental results, it can be found that the variation of e_{trans} to the burner position become more apparent when Φ = 3.0 for both cases of ID 40 and 50 mm (in the Φ-insensitive range). By comparing the results between cases of ID 40 and 50 mm, the change of tube ID shows less influence on e_{trans} than burner positions. It can be found that e_{trans} for the cases of 50 mm are greater than cases of 40 mm when Φ = 3.0, while the similar value of e_{trans} are obtained in the cases of Φ = 1.4. Therefore, both the influences of burner position and ID on the system deterministic nature at Φ = 3.0 validate that the decreases in heat release and overall flow rate might enhance the sensitivity of the system to the flow conditions around flame. In summary, the quantitative analysis of e_{trans} validates the findings obtained from the phase space diagram while providing more insightful information about the system deterministic nature.

3.3. Recurrence analysis

The results of phase space analysis show the system with remarkable deterministic natures, high periodicity and the absence of noticeable state transition in most cases. For such stable systems, the pattern of RP can be similar, and the result of RP might not be informative enough for the detailed analysis, as shown in Fig. 9 (a) (b) (c) and (e). Several clear continuous diagonal lines can be observed, which evidences the system with high periodicity and probability of occurrence of similar states. Slight differences between them still can be noticed, that the patterns for high periodic oscillation (Fig. 9 (a) (b)) have less scattered points, and the diagonal lines tend to be more gathered than lower periodic oscillation (Fig. 9 (c) (e)). However, the cases with quasi-periodic oscillation show noticeably different patterns, as shown in Fig. 9 (d) and (f). It can be found that the RPs of quasi-periodic oscillation present frequent pattern changes with different densities, which indicates the frequent shift of the system state. During the state shifting progress, the discontinuous diagonal lines can be observed as they are interrupted by the pattern changes due to the state changes. The existence of bowed structures in RP can be found as well, which implies the changing of system dynamics [39]. In order to further discover the recurrence properties of the system, RQA is applied to the results of RP to characterise the system nonlinear dynamics quantitatively, as shown in Fig. 10.

For the cases at L/4 of burner position and 40 mm of ID, slight differences of both RR and DET can be obtained when Φ and $\dot{m}_{CH_4}$ are changed. The values of DET for the cases at L/4 and ID 40 mm are found to be greater than 90%, indicating the considerable amount of diagonal structures in RPs [48]. The high value of DET (shown in Fig. 10 (b)) validates the finding from phase space analysis, that the system is more deterministic and less complex if the burner is at a higher position. Also, it is found that the values of ENT for the same cases are relatively small, which indicates the neglected chaoticity of system. From Fig. 10 (d), it can be seen that the ADL slightly increases with the increasing Φ, which shows the greater degrees of parallelism of the trajectory in phase space [38]. This trend indicates that the system state at higher Φ tends to be more sustainable with fewer interruptions. The more stable systems at higher Φ might be caused by the weakening flow instabilities due to lower overall flowrates at higher Φ but the same $\dot{m}_{CH_4}$. Thus, the oscillation can be less disturbed by the flow around flame. Under this circumstance, the probability of the system states being interrupted would be less, and the states would be more likely sustained.

The RQA results also validate the results of phase space analysis, that the system dynamics could be more easily affected by burner positions. It can be seen that all these measures become more sensitive to Φ changes when the burner is moved downwards (L/8, L/16) in the ID 40 mm system. The decreases in both RR and DET can be found when the burner is moved from L/4 to L/16. Meanwhile, both RR and DET of the cases at L/16 are significantly lower than those at L/4 and L/8, which indicates a more unstable and complex system at this position, as shown in Fig. 10 (a) (b). The results of DET generally conform to the results of e_{trans}, that the systems present considerable periodicity and deterministic nature if the burner is placed above L/8, while the system becomes more

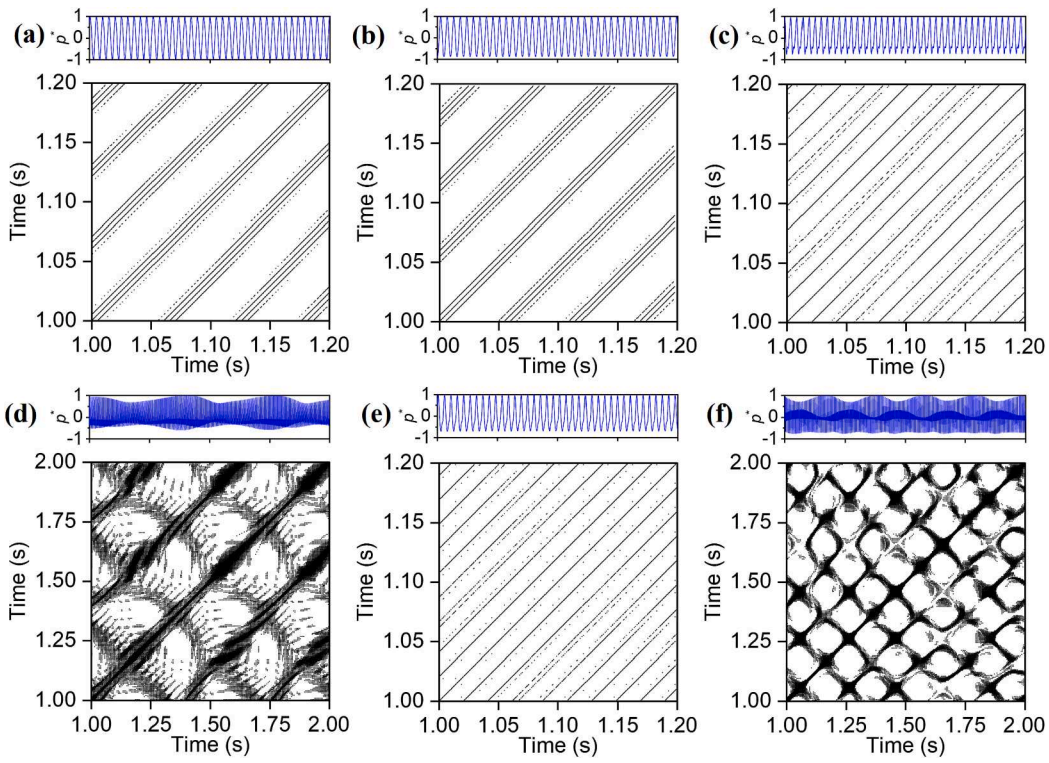

Fig. 9. RPs for the cases: (a) I. = 40 mm, L/4, $\dot{m}_{CH_4} = 0.65L/min$, $\Phi = 1.4$; (b) ID = 40 mm, L/4, $\dot{m}_{CH_4} = 0.65L/min$, $\Phi = 3.0$; (c) ID = 40 mm, L/16, $\dot{m}_{CH_4} = 0.65L/min$, $\Phi = 1.4$; (d) ID = 40 mm, L/16, $\dot{m}_{CH_4} = 0.65L/min$, $\Phi = 3$; (e) ID = 50 mm, L/16, $\dot{m}_{CH_4} = 0.65L/min$, $\Phi = 1.4$; (f) ID = 50 mm, L/16, $\dot{m}_{CH_4} = 0.65L/min$, $\Phi = 3$; The D = 3 is for all cases, τ is determined based on the first zero-crossing point method, $\varepsilon = 0.15\sigma$. The time-evolution of pressure fluctuations figures with normalised pressure oscillation amplitude (p^*) are shown above each RP.

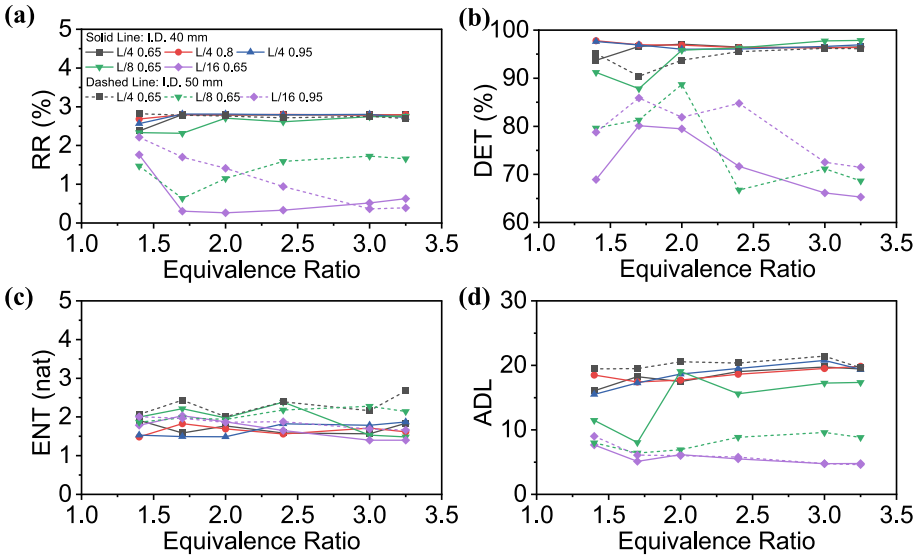

Fig. 10. The result of RQA at various Φ, burner positions, $\dot{m}_{CH_4}$, and tube ID The four figures represent (a) Recurrence Rate, (b) Determinism, (c) Shannon Entropy and (d) Average diagonal line length.

complex when the burner is at L/16. The low DET value of approximately 65% at L/16 of burner position implies fewer diagonal structures in RP and less occurrence of similar states. Meanwhile, the state can change more frequently in the system with low DET, such as the quasi-periodic oscillations (beating oscillations in this case). The ADL results show that the segments in trajectory tend to diverge faster at a lower burner position. The system state under this condition is more likely interrupted and less sustainable. However, the results of ENT show inapparent differences as the burner moved to a lower position. It implies that significant amounts of diagonal structures still exist in RP, although the system state is interrupted. Thus, the system becomes more complex when the burner is moved to a lower position, but the oscillation is still periodic with neglected chaoticity. The larger RR, DET and ADL at a higher burner position likely result from less disturbance in the region far from the lower tube end. Thus, the state of the nonlinear oscillations is more likely sustaining and has fewer state variations. In addition, RR, DET and ADL show greater sensitivities to the Φ changes at a lower burner position, which also indicates the significant state change due to the complex flow conditions around the lower tube end.

For the RQA results of 50 mm cases, similar findings can be concluded that a lower burner position might result into a system with higher complexity. Besides, by comparing the cases of both 40 and 50 mm ID, it is found that the inner diameter of the tube also is able to influence the system dynamics. The system becomes more complex

when the tube ID is increased to 50 mm, which is evidenced by a generally higher ENT of the 50 mm cases. In addition, for the cases at lower burner positions (L/8, L/16), the corresponding values of RR and DET also show apparent differences when the ID is changed. It further indicates that the flow condition around flame can be vital for characterising the dynamical properties of thermoacoustic oscillations since the flow condition can be more stable at the deeper position of tube. The influence of ID on the degrees of parallelism is found to be limited, which is implied by the minor changes in ADL values as the ID increases. By comparing the result between 40 and 50 mm ID cases, the results indicate that a more complex system can be generated if the chamber of the Rijke tube has a greater diameter. The experiments with more inner diameters will be conducted to verify such findings. In conclusion, it is proved that the system parameters investigated in this study are effective for changing the system nonlinear dynamics to varying extents, and the burner position presents a more decisive role in influencing the system.

4. Conclusions

In this study, the effects of system parameters on characterising the self-excited thermoacoustic oscillation in a Rijke tube were experimentally investigated. The results of both oscillation amplitude and system frequency response were obtained based on the measured pressure signals. Multiple analysis methods were applied to quantify the system characteristics under different system conditions. More specifically, the phase space analysis based on the time-delayed embedding method successfully indicated the system stability, and the variety of periodic and quasi-periodic attractors was observed. The calculation of translation error for the trajectory in phase space quantitatively determined the system deterministic nature. The recurrence analysis effectively and directly investigated the recursiveness of a nonlinear thermoacoustic system from the time-domain.

It has been found that the system parameters investigated in this study significantly influence the eigenfrequency of thermoacoustic oscillations, the complexity and the periodicity of the system. The findings for the effect of system parameters which were investigated in this study can be summarised as followings:

- Both the Φ-insensitive range and Φ-sensitive range were found. The system frequency response presented different sensitivity to equivalence ratio changes at a constant fuel flowrate. The eigenfrequency in the Φ-sensitive range was greater than in the Φ-insensitive range.
- In Φ-insensitive range, the quasi-linear relationship between fuel flowrate and mean stable eigenfrequency can be highlighted. The quasi-linear trends had similar increasing rates, regardless of the system parameter change.
- The eigenfrequencies were inversely proportional to burner positions and tube inner diameter. A simplified model for validating the discussions about the lower eigenfrequency obtained in a larger diameter tube was developed. The change in average sound speed due to the mean temperature change was found as the main reason for eigenfrequency changes.
- It was found that the increasing equivalence ratio would increase the deterministic natures and decrease the complexity of system if the quasi-periodic oscillation was not triggered.
- Burner position could change the system dynamics to a larger extent. A more complex and unstable system with less deterministic natures was likely generated if the burner was at a lower position. The system states also were more easily affected by the changes of equivalence ratio at lower burner positions.
- The influence of tube inner diameter on characterising the system was obtained by the variation of system dynamics. However, the experiments at the tubes of more different inner diameters should be conducted in the future to quantify the effect of tube inner diameter on system nonlinear dynamics.

This study shows the critical roles of different system parameters on the self-excited thermoacoustic oscillation in the Rijke tube. It has been proved that the analysis methods utilised in this study are effective for quantifying the nonlinear characteristics of the thermoacoustic system in time-domain, which are also applicable to various combustion systems with nonlinear characteristics.

CRediT authorship contribution statement

Xuanqi Liu: Conceptualization, Methodology, Software, Formal analysis, Investigation, Writing – original draft, Visualization. **Hangxu Zhou:** Validation, Writing – review & editing, Formal analysis, Investigation. **Yufeng Lai:** Validation, Resources, Writing – review & editing, Investigation. **Yang Zhang:** Supervision, Writing – review & editing.

Declaration of Competing Interest

The authors declare that they have no known competing financial interests or personal relationships that could have appeared to influence the work reported in this paper.

Data availability

Data will be made available on request.

Acknowledgement

The authors wish to acknowledge the Transforming Foundation Industries Network+ (EPSRC grant EP/V026402/1) for partly funding this work.

References

[1] C.J. Lawn, G. Penelet, Common features in the thermoacoustics of flames and engines, Int. J. Spray. Combust. Dynam. 10 (2018) 3–37, https://doi.org/10.1177/1756827717743911.
[2] N.M. Hariharan, P. Sivashanmugam, S. Kasthurirengan, Influence of stack geometry and resonator length on the performance of thermoacoustic engine, Appl. Acoust. 73 (2012) 1052–1058, https://doi.org/10.1016/j.apacoust.2012.05.003.
[3] Y. Guan, P. Liu, B. Jin, V. Gupta, L.K.B. Li, Nonlinear time-series analysis of thermoacoustic oscillations in a solid rocket motor, Exp. Therm. Fluid. Sci. 98 (2018) 217–226, https://doi.org/10.1016/j.expthermflusci.2018.06.002.
[4] H. Kobayashi, H. Gotoda, S. Tachibana, Nonlinear determinism in degenerated combustion instability in a gas-turbine model combustor, Physica. A 510 (2018) 345–354, https://doi.org/10.1016/j.physa.2018.06.024.
[5] P. Novotný, T. Vít, M. Vestfálová, J. Lopes, Standing-wave thermoacoustic engines, EPJ. Web. Conf. 25 (2012) 01061, https://doi.org/10.1051/epjconf/20122501061.
[6] Y. Huang, V. Yang, Bifurcation of flame structure in a lean-premixed swirl-stabilized combustor: transition from stable to unstable flame, Combust. Flame. 136 (2004) 383–389, https://doi.org/10.1016/j.combustflame.2003.10.006.
[7] H. Zhao, G. Li, D. Zhao, Z. Zhang, D. Sun, W. Yang, S. Li, Z. Lu, Y. Zheng, Experimental study of equivalence ratio and fuel flow rate effects on nonlinear thermoacoustic instability in a swirl combustor, Appl. Energy. 208 (2017) 123–131, https://doi.org/10.1016/j.apenergy.2017.10.061.
[8] M.P. Juniper, R.I. Sujith, Sensitivity and Nonlinearity of Thermoacoustic Oscillations, Annu. Rev. Fluid. Mech. 50 (2018) 661–689, https://doi.org/10.1146/annurev-fluid-122316-045125.
[9] D. Ebi, A. Denisov, G. Bonciolini, E. Boujo, N. Noiray, Flame Dynamics Intermittency in the Bistable Region Near a Subcritical Hopf Bifurcation, J. Eng. Gas. Turbine. Power. 140 (2018), https://doi.org/10.1115/1.4038326.
[10] B. Zhang, M. Shahsavari, Z. Rao, S. Yang, B. Wang, Thermoacoustic instability drivers and mode transitions in a lean premixed methane-air combustor at various swirl intensities, in: Proceedings of the Combustion Institute, Elsevier Ltd, 2021: pp. 6115–6124. https://doi.org/10.1016/j.proci.2020.06.226.
[11] K.R. McManus, T. Poinsot, S.M. Candel, A review of active control of combustion instabilities, Prog. Energy. Combust. Sci. 19 (1993) 1–29, https://doi.org/10.1016/0360-1285(93)90020-F.
[12] R.L. Raun, M.W. Beckstead, J.C. Finlinson, K.P. Brooks, A review of Rijke tubes, Rijke burners and related devices, Prog. Energy. Combust. Sci. 19 (1993) 313–364, https://doi.org/10.1016/0360-1285(93)90007-2.
[13] T.C. Lieuwen, Vigor. Yang, Combustion instabilities in gas turbine engines : operational experience, fundamental mechanisms and modeling, American Institute of Aeronautics and Astronautics, 2005.
[14] Rayleigh, The explanation of certain acoustical phenomena 1, Nature. 18 (1878) 319–321. https://doi.org/10.1038/018319a0.

[15] N. Swaminathan, G. Xu, A.P. Dowling, R. Balachandran, Heat release rate correlation and combustion noise in premixed flames, J. Fluid. Mech. 681 (2011) 80–115, https://doi.org/10.1017/jfm.2011.232.
[16] K. Balasubramanian, R.I. Sujith, Thermoacoustic instability in a Rijke tube: Non-normality and nonlinearity, in: Physics of Fluids, American Institute of Physics Inc., 2008. https://doi.org/10.1063/1.2895634.
[17] J. O'Connor, V. Acharya, T. Lieuwen, Transverse combustion instabilities: Acoustic, fluid mechanic, and flame processes, Prog. Energy. Combust. Sci. 49 (2015) 1–39, https://doi.org/10.1016/j.pecs.2015.01.001.
[18] F. Weng, S. Li, D. Zhong, M. Zhu, Investigation of self-sustained beating oscillations in a Rijke burner, Combust. Flame. 166 (2016) 181–191, https://doi.org/10.1016/j.combustflame.2016.01.016.
[19] D. Zhao, Z.H. Chow, Thermoacoustic instability of a laminar premixed flame in Rijke tube with a hydrodynamic region, J. Sound. Vib. 332 (2013) 3419–3437, https://doi.org/10.1016/j.jsv.2013.01.031.
[20] M.P. Juniper, Triggering in the horizontal Rijke tube: Non-normality, transient growth and bypass transition, J. Fluid. Mech. 667 (2011) 272–308, https://doi.org/10.1017/S0022112010004453.
[21] M.A. Heckl, M.S. Howe, Stability analysis of the Rijke tube with a Green's function approach, J. Sound. Vib. 305 (2007) 672–688, https://doi.org/10.1016/j.jsv.2007.04.027.
[22] J.A. Carvalho, M.A. Ferreira, C. Bressan, J.L.G. Ferreira, Definition of heater location to drive maximum amplitude acoustic oscillations in a Rijke tube, Combust. Flame. 76 (1989) 17–27, https://doi.org/10.1016/0010-2180(89)90073-4.
[23] N.N. Deshmukh, S.D. Sharma, Experiments on heat content inside a Rijke tube with suppression of thermo-acoustics instability, Int. J. Spray. Combust. Dynamics. 9 (2017) 85–101, https://doi.org/10.1177/1756827716655007.
[24] D. Zhao, Transient growth of flow disturbances in triggering a Rijke tube combustion instability, Combust. Flame. 159 (2012) 2126–2137, https://doi.org/10.1016/j.combustflame.2012.02.002.
[25] M. Fleifil, Response of a laminar premixed flame to flow oscillations: A kinematic model and thermoacoustic instability results, Combust. Flame. 106 (1996) 487–510, https://doi.org/10.1016/0010-2180(96)00049-1.
[26] H. Gotoda, H. Nikimoto, T. Miyano, S. Tachibana, Dynamic properties of combustion instability in a lean premixed gas-turbine combustor, Chaos 21 (2011), https://doi.org/10.1063/1.3563577.
[27] C. Tao, H. Zhou, Effects of operating parameters on the combustion oscillation behaviour in a lean premixed CH4 combustor, J. Mech. Sci. Technol. 35 (2021) 3753–3762, https://doi.org/10.1007/s12206-021-0744-4.
[28] X. Han, D. Laera, A.S. Morgans, C.J. Sung, X. Hui, Y.Z. Lin, Flame macrostructures and thermoacoustic instabilities in stratified swirling flames, Proceedings of the Combustion Institute. 37 (2019) 5377–5384. https://doi.org/10.1016/j.proci.2018.06.147.
[29] T. Lieuwen, B.T. Zinn, The role of equivalence ratio oscillations in driving combustion instabilities in low NOx gas turbines, Symp. (Int.). Combust. 27 (1998) 1809–1816, https://doi.org/10.1016/S0082-0784(98)80022-2.
[30] S.J. Shanbhogue, Y.S. Sanusi, S. Taamallah, M.A. Habib, E.M.A. Mokheimer, A. F. Ghoniem, Flame macrostructures, combustion instability and extinction strain scaling in swirl-stabilized premixed CH 4 /H 2 combustion, Combust. Flame. 163 (2016) 494–507, https://doi.org/10.1016/j.combustflame.2015.10.026.
[31] Y. Guan, V. Gupta, L.K.B. Li, Intermittency route to self-excited chaotic thermoacoustic oscillations, J. Fluid. Mech. 894 (2020), https://doi.org/10.1017/jfm.2020.297.
[32] S. Tandon, R.I. Sujith, Condensation in the phase space and network topology during transition from chaos to order in turbulent thermoacoustic systems, Chaos 31 (2021), https://doi.org/10.1063/5.0039229.
[33] R. Wayland, D. Bromley, D. Pickett, A. Passamante, Recognizing determinism in a time series, Phys. Rev. Lett. 70 (1993) 580–582, https://doi.org/10.1103/PhysRevLett.70.580.
[34] Y. Hirata, S. Horai, H. Suzuki, K. Aihara, Testing serial dependence by Random-shuffle surrogates and the Wayland method, Phys. Lett. A. 370 (2007) 265–274, https://doi.org/10.1016/j.physleta.2007.05.061.
[35] D.T. Kaplan, L. Glass, Direct test for determinism in a time series, Phys. Rev. Lett. 68 (1992) 427–430, https://doi.org/10.1103/PhysRevLett.68.427.
[36] R. Hernandez-Rivera, G. Troiani, T. Pagliaroli, A. Hernandez-Guerrero, Detection of the thermoacoustic combustion instabilities of a slot burner based on a diagonal-wise recurrence quantification, Phys. Fluids 31 (2019), 124105, https://doi.org/10.1063/1.5124015.
[37] V. Nair, R.I. Sujith, Intermittency as a Transition State in Combustor Dynamics: An Explanation for Flame Dynamics Near Lean Blowout, Combust. Sci. Technol. 187 (2015) 1821–1835, https://doi.org/10.1080/00102202.2015.1066339.
[38] M. Murugesan, S. Balusamy, S. Hochgreb, L.K.B. Li, Recurrence analysis of forced synchroniza-tion in a self-excited thermoacoustic system, 24th International Congress on Sound and Vibration, ICSV 2017 (2017). 10.17863/CAM.33084.
[39] N. Marwan, M. Carmenromano, M. Thiel, J. Kurths, Recurrence plots for the analysis of complex systems, Phys. Rep. 438 (2007) 237–329, https://doi.org/10.1016/j.physrep.2006.11.001.
[40] G.S. Samuelsen, J. Brouwer, M.A. Vardakas, J.D. Holdeman, Experimental and modeling investigation of the effect of air preheat on the formation of NOx in an RQL combustor, Heat. Mass. Transf. 49 (2013) 219–231, https://doi.org/10.1007/s00231-012-1080-0.
[41] A.P. Dowling, The calculation of thermoacoustic oscillations, J. Sound. Vib. 180 (1995) 557–581, https://doi.org/10.1006/JSVI.1995.0100.
[42] F. Takens, Detecting strange attractors in turbulence, in: 1981: pp. 366–381. https://doi.org/10.1007/BFb0091924.
[43] L. Kabiraj, A. Saurabh, P. Wahi, R.I. Sujith, Route to chaos for combustion instability in ducted laminar premixed flames, Chaos 22 (2012), https://doi.org/10.1063/1.4718725.
[44] L.P. Yang, S.L. Ding, G. Litak, E.Z. Song, X.Z. Ma, Identification and quantification analysis of nonlinear dynamics properties of combustion instability in a diesel engine, Chaos 25 (2015), https://doi.org/10.1063/1.4899056.
[45] S. Schinkel, O. Dimigen, N. Marwan, Selection of recurrence threshold for signal detection, Eur. Phys. J. Spec. Top. 164 (2008) 45–53, https://doi.org/10.1140/epjst/e2008-00833-5.
[46] R. Hernandez-Rivera, T. Pagliaroli, G. Troiani, A. Hernandez-Guerrero, Early detection of the combustion instabilities by quantifying diagonal-wise measurements of joint recurrence plots of pressure and radiant energy fluctuations, Phys. Fluids 34 (2022), 044113, https://doi.org/10.1063/5.0086658.
[47] H. Zan, W. Zhou, X. Xiao, L. Lin, J. Zhang, H. Li, Recurrence network analysis for uncovering dynamic transition of thermo-acoustic instability of supercritical hydrocarbon fuel flow, Aerosp. Sci. Technol. 85 (2019) 1–12, https://doi.org/10.1016/j.ast.2018.11.040.
[48] N. Marwan, How to avoid potential pitfalls in recurrence plot based data analysis, Int. J. Bifurcation. Chaos 21 (2011) 1003–1017, https://doi.org/10.1142/S0218127411029008.
[49] T. Braun, V.R. Unni, R.I. Sujith, J. Kurths, N. Marwan, Detection of dynamical regime transitions with lacunarity as a multiscale recurrence quantification measure, Nonlinear. Dyn. 104 (2021) 3955–3973, https://doi.org/10.1007/s11071-021-06457-5.
[50] X. Liu, H. Zhou, Y. Lai, Y. Zhang, Equivalence ratio independence and dependence ranges of system responses for a nonlinear thermoacoustic oscillation in a Rijke tube, J. Sound. Vib. (2022), 117545, https://doi.org/10.1016/j.jsv.2022.117545.
[51] R.I. Sujith, S.A. Pawar, Thermoacoustic Instability, Springer International Publishing, Cham (2021), https://doi.org/10.1007/978-3-030-81135-8.
[52] D. You, Y. Huang, V. Yang, A generalized model of acoustic response of turbulent premixed flame and its application to gas-turbine combustion instability analysis, Combustion Science and Technology, in, 2005, pp. 1109–1150.
[53] S.R. Turns, An Introduction to Combustion: Concepts and Applications, third ed., McGraw-Hill, New York, 2011.
[54] R. Friedman, E. Burke, Measurement of temperature distribution in a low-pressure flat flame, J. Chem. Phys. 22 (1954) 824–830, https://doi.org/10.1063/1.1740197.
[55] C.K. Law, Combustion Physics, Cambridge University Press (2006), https://doi.org/10.1017/CBO9780511754517.
[56] F.A. Williams, Combustion Theory, CRC. Press (2018), https://doi.org/10.1201/9780429494055.
[57] K. Kashinath, I.C. Waugh, M.P. Juniper, Nonlinear self-excited thermoacoustic oscillations of a ducted premixed flame: Bifurcations and routes to chaos, J. Fluid. Mech. 761 (2014) 399–430, https://doi.org/10.1017/jfm.2014.601.